Vol. 14, No. 41, Winter 2025, pages 43-54

Journal of Analytical and Numerical Methods in Mining Engineering

Journal home page: http://anm.yazd.ac.ir/

Research article

An investigation into the performance of bottom air-deck method in the presence of water, using SPH-FEM

Mehrdad Moradi[1], Mohamad Ali Ebrahimi Farsangi[1]*, Hamid Mansour[1], Mohsen Saffari Pour[2]

1- Dept. of Mining Engineering, Shahid Bahonar University of Kerman, Kerman, Iran
2- Dept. of Mechanical Engineering, Shahid Bahonar University of Kerman, Kerman, Iran

*Corresponding author: E-mail: *maebrahimi@uk.ac.ir*

(Received: *April 2024*, Accepted: *January 2025*)

DOI: 10.22034/ANM.2025.21431.1631

Keywords

SPH-FEM
Air-Deck
Water-Deck
Rock blasting
LS-Dyna

Abstract

The use of the bottom air-deck method in open-pit blasting has been widely accepted by researchers as an efficient technique. In this method, leaving an empty space (air-deck) at the bottom of the blast hole improves the blast results. However, if the blast hole is filled with water, the presence of water may affect the blast results. In such cases, it is necessary to study the effect of the water in the air-deck area on blasting performance. In this research, a numerical method was used to investigate the effect of the presence of water in the blast hole on the blasting results in the bottom air-deck method. Considering the advantages of the SPH method in modeling the fractures caused by blasting and the advantage of the FEM method in terms of processing time, the combined SPH-FEM method was used to carry out the simulation. The Dehghan-Banadki empirical model was employed to validate the model and determine the SPH parameters. The results showed that due to the incompressibility of water, more pressure produced by the explosive detonation is transferred to the rock, Additionally, water causes attenuation of the blast wave and reduces the wave frequency. In a dry blast hole, despite the decrease in the initial wave pressure compared to a water-filled blast hole, multiple reflections of the wave in the empty space lead to longer duration waves and absorption of explosive energy by the rock. The peak effective stress taken at different distances around the blast hole in the air-deck area showed that the maximum stress applied to the rock in the water-filled blast hole is higher. The results also indicated that the total length of fractures in the dry blasting condition is 13.15 m, while in the water-filled blast hole blasting, it is 12.5 m. Therefore, the total length of fractures in the dry blast hole is only 5% more than in the water-filled blast hole. In other words, the presence of water in the air-deck area does not have a negative effect on the blasting results, and thus, this method can also be used in water-filled blast holes.

1. INTRODUCTION

In open-pit mining, drilling, and blasting costs constitute approximately 30-40% of the total unit production costs. Studies have shown that only 15-20% of the explosive energy is effectively used for rock fragmentation, with the remaining energy being dissipated as ground vibrations, air blasts, fly rock, back break, and other detrimental effects [1, 2]. Consequently, the adopting methods to optimize the blasting process can significantly reduce mining costs, mitigate adverse environmental impacts, and increase overall profitability.

Researchers have demonstrated that leaving a void at the bottom of the blast hole (bottom air deck) enhances fragmentation, reduces toe problems, and minimizes the adverse effects of blasting, such as ground vibrations, fly rock, air blast, back break, and boulders. Additionally, the utilization of the bottom air deck method can eliminate or reduce sub-drilling and explosive

consumption [3-5]. Ultimately, these improvements lead to a decrease in mine production costs.

Numerous researchers have extensively investigated the application of bottom air-deck. Rollmandz (1989) examined the utilization of air-deck blasting method in a coal mine. This study demonstrated that air-deck lengths of 0.28 to 0.36 times the main charge are suitable for soft rock. Moreover, the employment of the air-deck blasting method led to a reduction in explosive consumption, accompanied by a 15-20% decrease in rock fragment size [6]. Korea and colleagues (2003) employed the bottom air-deck blasting method at the Escondido open-pit mine. The results indicated improved rock fragmentation without any adverse effects. Additionally, the utilization of the bottom air-deck decreased specific charges and eliminated the need for over-drilling in this mine [7]. Chiapetta (2004) demonstrated that the application of a bottom air-deck in open-pit mine blasting resulted in a reduction of ground vibration by approximately 33%, a decrease in specific charge of around 16-25%, and an increase in fragmentation by up to 25% [8].

Furthermore, Floyd (2004) applied the bottom air-deck blasting method at a gold open-pit mine in Northern Nevada. The results demonstrated a 31% reduction in specific charge and a decrease in drilling without adverse effects. Ultimately, the annual mining cost reduction resulting from the implementation of this method was calculated to be approximately $966,240 [9]. Additionally, Askari et al. (2018) utilized the bottom air-deck blasting method at the Gohrzemin iron ore mine, Iran, to eliminate adverse blast results such as toe problems, and air blasts, while improving rock fragmentation. Applying this method not only enhanced blasting results but also led to a 15% decrease in blasting costs [10]. Moreover, Zarei et al. (2022) investigated the application of the bottom air-deck blasting method at the Anguran lead-zinc mine, in Iran. The results indicated that this method improved fragmentation, resolved toe problems, and reduced fly rock [11].

While most studies have demonstrated that the application of the bottom air-deck enhances blasting results, the performance of the blast may be compromised if the air-deck area is filled with water due to hydrogeological conditions. The impact of water presence in the air-deck area on blasting performance and its results has not been investigated. This research examines the performance of the bottom air-deck blasting method under water-filled blast hole conditions using numerical methods. To this end, the distribution of blast-induced stresses around the blast hole and the resulting fractures are studied to evaluate the performance of the bottom air-deck in both dry and water-filled blast holes.

Various numerical methods have been employed to model rock mass blasting and the propagation of blast-induced fractures in rock masses. These methods include mesh-based methods such as the finite element method (FEM) [12], the extended finite element method (XFEM) [13], and the discrete element method (DEM) [14], as well as mesh-free methods such as the discrete element method with cracking [15]-[18] and the smoothed particle hydrodynamics method (SPH) [19], and finally hybrid methods such as FEM-DEM [20], DEM-SPH [21], and FEM-SPH [22], [23].

In complex problems such as blast-induced crack propagation, the use of mesh-based methods is associated with challenges. Numerical methods based on meshing have limitations for modeling crack propagation [24]. In the FEM, when a crack propagates in the model, the entire model geometry must be modified, which requires re-meshing the whole model [24]. Moreover, re-meshing is performed, using complex techniques, however, it is impractical for complex fracture networks. In this method, crack propagation is achieved, using an erosion algorithm where elements reaching a critical stress level are removed [25]. It is worth noting that DEM and XFEM methods are also used for modeling crack propagation. A significant point is that in the XFEM method, crack tips are always located at element boundaries and propagate along nodes. Therefore, the accuracy of crack propagation, using this method depends on the mesh size, and if a coarse mesh is used, crack initiation and propagation will not be accurately represented [13].

All blasting processes exhibit fundamental characteristics such as large deformations, high heterogeneity, evolving boundaries, and free surfaces. These fundamental characteristics pose significant challenges in numerical simulations, using mesh-based methods. Therefore, simulating the blasting process, using continuum methods is often not the optimal choice [26].

Mesh-free methods, owing to their ability to circumvent the need for re-meshing, offer efficient numerical approaches for modeling crack propagation. Monaghan et al. (1977) introduced and developed the smoothed particle hydrodynamics (SPH) method. In this method, each particle interacts with its neighboring particles based on an interpolation equation [27]. Given its Lagrangian and mesh-free nature, this method is well-suited for problems involving large

deformations such as crack propagation, rock fragmentation, and rock fracture [28].

Compared to mesh-based numerical methods, mesh-free numerical methods such as SPH generally exhibit higher computational costs. Consequently, hybrid approaches combining mesh-based and mesh-free methods have garnered significant attention due to their ability to leverage the strengths of both techniques. Mesh-free methods are well-suited for modeling crack propagation, while mesh-based methods are often preferred for their lower computational cost [22], [29], [30].

Many researchers have employed hybrid approaches combining mesh-based and mesh-free numerical methods to simulate crack propagation. Fakhimi et al. (2014) utilized a combined DEM-SPH method to investigate the impact of blast-induced gases on crack propagation [20]. Furthermore, Hu et al. (2015) adopted a hybrid approach involving SPH, a modified damage model, and FEM to numerically simulate the complete response of rock masses to blasting within the LS-Dyna software. In their model, regions near the blast, subjected to the highest stresses, were modeled, using SPH and a modified damage model. For regions farther from the blast, subjected to lower stresses, the FEM was employed [31].

Gharehdash et al. (2016) modeled the rock mass response to blasting, using the LS-Dyna software, employing a combined SPH-FEM method. In this study, the SPH method was utilized to model fractured zones around the blast hole, while the FEM was applied to model the influenced regions. The results demonstrated the effectiveness of the SPH-FEM combination in simulating rock mass failure induced by blasting [32]. Additionally, Wang et al. (2020) utilized a combined SPH-FEM method to model blast-induced fractures. The findings of this research indicated that the combined SPH-FEM method offers superior advantages over standalone FEM and SPH methods for simulating blast-induced fractures [33].

As previously mentioned, this research investigates the performance of the bottom air-deck blasting method in both wet and dry blast holes. The results obtained from wet blast holes are compared with those from dry blast holes. Given the advantages of the combined SPH-FEM method, this approach is employed for numerical modeling, using the LS-Dyna software.

2. AİR-DECK BLASTİNG MECHANİSM

In a typical rock blasting, the pressure generated from the blast is applied to the rock mass as a high-velocity shockwave, inducing the formation and propagation of fractures within the rock. The expansion of gases further widens these blast-induced fractures, contributing to increased fracturing and fragmentation of the rock mass. In the vicinity of the blast hole, the pressure exerted on the rock mass exceeds the rock's strength, resulting in excessive rock failure around the blast hole [34], [35].

In air-deck blasting, incorporating a void along the blast hole reduces explosive consumption and ensures uniform energy distribution and optimized utilization of explosive energy. In this method, blast products such as shockwaves and detonation gases expand into the void upon detonation. This reduces the initial blast pressure. However, the shockwave becomes trapped within the void and is applied to the rock mass in multiple pulses (Fig. 1) [5]. The pressure wave oscillates within the void and is reflected as a tension wave. The repeated impact of the wave on the rock mass within the air deck area and the generation of secondary waves increase the duration of wave application to the rock mass. In air-deck blasting, the energy imparted to the rock mass is 1.5 to 1.7 times greater than that in conventional blasting, significantly enhancing rock fragmentation [34].

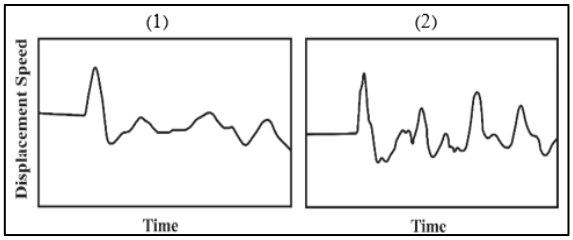

Fig. 1. Rock displacement speed due to blasting. 1) Conventional blasting, 2) Air-deck blasting

The location of the air-deck in the air-deck blasting method is crucial and significantly influences blast results. Researchers have generally proposed three positions for the air-deck: above the blast hole and below the stemming, in the middle of the blast hole, and at the bottom of the blast hole (Fig. 2) [36]. Middle air-deck blasting, due to the collision of two wave fronts in the middle of the air-deck area, exhibits superior rock fragmentation performance compared to initial and final air-deck blasting [37]. On the other hand, in top air-deck blasting, the interaction of the shockwave in this region results in uniform energy distribution and effective fragmentation within the stemming zone. Additionally, in bottom air-deck blasting, the wave

interaction at the blast hole bottom and the generation of secondary waves enhance rock fragmentation in this area [5].

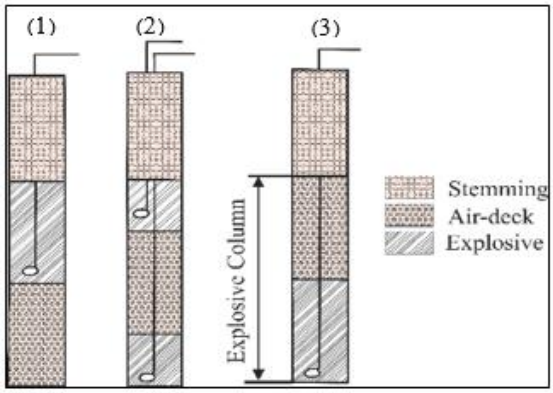

Fig. 2. Air-deck location. 1) Bottom air-deck, 2) Middle air-deck, 3) Top air-deck

3. SPH METHOD

The Smoothed Particle Hydrodynamics (SPH) method was initially developed and applied to astrophysical problems [38]. However, due to its Lagrangian nature (dividing the entire model into particles and independent units with their specific properties) and simplicity of use, it has attracted significant attention from researchers for applications in fluid and solid mechanics [39]. The SPH method utilizes interpolation and the smoothing property of the Dirac delta function. In this method, the computational domain is divided into a number of particles. Each particle has its unique properties and interacts with other particles. In the SPH method, the support domain of each particle is a region where particles within this region influence that particle [27], [40].

The integral concept of function f(x) in the SPH method is represented by Equation (1) [41].

$$f(x) = \int_{\Omega} f(x')\delta(x - x')dx' \tag{1}$$

Where Ω is the volume of integration. f(x') is the three-dimensional function of the position vector x and δ (x-x') is the delta-Dirac function, which is equal to:

$$\delta(x - x') = \begin{cases} 1 & x = x' \\ 0 & x \neq x' \end{cases} \tag{2}$$

On the other hand, in Equation 1, if δ (x-x') is replaced with a smoothing function of $w(x - x', h)$, the integral representation of the function f(x) is as follows:

$$f(x) = \int_{\Omega} f(x')w(x - x', h)dx' \tag{3}$$

Where w is the smoothing function or kernel function. In this relation h is the support domain which represents the range of influence of the function w. The kernel function W is expressed as follows:

$$W(x, h) = \frac{1}{h(x)^d}\,\theta(x) \tag{4}$$

Where d is the number of spatial dimensions and h is the smoothing length, which varies with time and space. The cubic B-Spline smoothing kernel function (θ(x)) is the most commonly used function in the SPH method.

$$\theta(x) = C \times \begin{cases} 1 - \frac{3}{2}u^2 + \frac{3}{4}u^3 & |u| \leq 1 \\ \frac{1}{4}(2 - u)^3 & |u| \leq 2 \\ 0 & |u| > 2 \end{cases} \tag{5}$$

Where C is a constant for normalizing the function, which depends on the number of dimensions of the space. u is the normalized distance between particles ($u = \frac{x_i - x_j}{h}$). If Equation 1 is converted to a sum, the discrete estimation function becomes the sum of the properties of the neighboring particles of particle i:

$$\langle f(x)\rangle \cong \sum_{j=1}^{n} \frac{m_j}{\rho_j} f(x_j)W(x - x_j, h) \tag{6}$$

Where n is the number of particles in the support domain, m_j is the mass of particle j, and ρ_j is the density of particle j. The transformation of the continuum mechanics conservation equations into the SPH discrete particle equations is shown below:

$$\frac{d\rho_i}{dt} = \rho_i \sum_j \frac{m_j}{\rho_j}(u_j - u_i).\nabla_i W_{ij} \tag{7}$$

$$\frac{du_i}{dt} = \sum_j m_j\left(\frac{\sigma_i}{\rho_i^2} + \frac{\sigma_j}{\rho_j^2}\right).\nabla_i W_{ij} \tag{8}$$

$$\frac{de_i}{dt} = \frac{1}{2}\sum_j m_j(u_j - u_i).\left(\frac{\sigma_i}{\rho_i^2} + \frac{\sigma_j}{\rho_j^2}\right).\nabla_i W_{ij} \tag{9}$$

In the above equations, density (ρ), internal energy (e), velocity vector (u) and stress tensor (σ) are the dependent variables. The spatial position of particle x and time t are the independent variables. Equations (5) to (7) represent the density, velocity and change in internal energy of particle i, respectively [25].

3.1. SPH Parts Interaction

In the SPH method, if the properties of two SPH parts differ significantly, incorrect particle properties may be calculated during the SPH

smoothing process [42]. This problem can be solved using a penalty-based contact model. In this contact model, contact is first detected, and then a repulsive force is applied to prevent interpenetration between the two regions. To detect penetration, the distance between two particles from different parts is first calculated and then compared with the smoothing length. Penetration between two SPH parts is defined as follows [43].

$$pe = \frac{2h_i + 2h_j}{r_{ij}} \geq 1 \quad (10)$$

Where r_{ij} represents the distance between two particles i and j. pe represents the penetration between two particles i and j. 2hi and 2hj represent the smoothing lengths of particles i and j.

After identifying the penetration between two particles, a contact repulsive force is applied to the particles equal to Equation 11.

$$f_i = \begin{cases} K_p \sum_{j=1}^{n} \frac{m_j}{\rho_i \rho_j} W_{ij} \frac{x_{ij}}{r_{ij}^2} & pe \geq 1 \\ 0 & pe < 1 \end{cases} \quad (11)$$

In this equation, Kp is the contact penalty force scaling factor, which determines the magnitude of the contact force. This coefficient is a dimensionless scalar parameter. In the LS-Dyna software, the *DEFINE_SPH_TO_SPH_COUPLING command is used to solve contact problems between two SPH particles [44].

3.2. Artificial Viscosity

Significant discontinuities can arise in the SPH simulations due to impulsive and shock loading within the model. These phenomena can lead to substantial non-physical oscillations and numerical instability in the momentum and energy equations (Equations 8 and 9). Adding an artificial viscosity term to the momentum and energy equations can mitigate this issue [45].

This study employed the artificial viscosity proposed by Gingold and Monaghan [27].

$$\Pi_{ij} = \begin{cases} \frac{-\alpha \bar{c}_{ij} \lambda_{ij} + \beta \lambda_{ij}^2}{\bar{\rho}_{ij}} & u_{ij}.x_{ij} < 0 \\ 0 & u_{ij}.x_{ij} \geq 0 \end{cases} \quad (12)$$

$$\lambda_{ij} = \frac{h_{ij} u_{ij}.x_{ij}}{|x_{ij}|^2 + 0.01h^2} \quad (13)$$

$$\bar{c}_{ij} = \frac{1}{2}(c_i + c_j) \quad (14)$$

$$\bar{\rho}_{ij} = \frac{1}{2}(\rho_i + \rho_j) \quad (15)$$

$$h_{ij} = \frac{1}{2}(h_i + h_j) \quad (16)$$

$$u_{ij} = (u_i - u_j) \quad (17)$$

$$x_{ij} = (x_i - x_j) \quad (18)$$

Where α (linear viscosity) and β (quadratic viscosity) are constants, and c is the speed of sound in the material. The quadratic viscosity term, β, is predominantly dominant in models subjected to high loading conditions, such as shock loading, while the linear viscosity term is dominant in low gradient loading conditions [46].

3.3. SPH-FEM Coupling

A coupling SPH-FEM method was employed for the numerical modeling of the air-deck blasting method. In this approach, SPH was utilized for regions near the blast hole, which experienced significant deformation and fracturing. On the other hand, FEM was used to model regions farther away from the blast, characterized by considerably less fracturing. In this method, information is transferred between the SPH and FEM domains at their interface. This hybrid approach provides an efficient, accurate, and cost-effective method for modeling the complete rock mass response to blasting, including fragmentation, fracturing, and displacement induced by the blast [44].

The coupling of SPH particles and conventional FEM meshes has been achieved through the implementation of three distinct methods [47]. One approach to coupling SPH particles and FEM meshes is to tie the SPH particles to the corresponding surfaces of the FEM meshes (Fig. 3-1). If the SPH particles are not coupled to the FEM mesh through surface tying, as depicted in Fig. 3-2, their interaction is established through contact between penalty-based nodes and the surface. The hybrid elements are utilized as intermediary layers between the SPH particles and FEM meshes in the third approach, as illustrated in Fig. 3-3. In this study, the tied interface shown in Fig. 3a was used to couple the SPH and FEM methods.

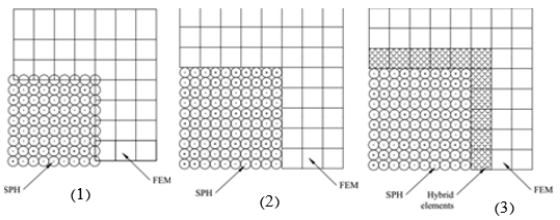

Fig. 3. Coupling SPH-FEM methods. 1) Tied interface, 2) nodes-to-surface contact, 3) hybrid elements [47].

4. MODEL GEOMETRY

The model comprised a 6 m deep blast hole with a 150 mm diameter, 1.5 m stemming, 3.7 m charge length, 80 cm air-deck or water-deck column, and a TNT explosive charge.

Extensive research has been conducted to determine the optimal length of the air-deck in blast holes. Jhanwar (1998) suggested that for hard rocks, an air-deck length equal to 0.18 times the original charge length is suitable [48]. Therefore, for an original charge length of 4.5 meters, an air-deck length of 80 cm is appropriate.

The SPH method was employed within the LS-Dyna software to model the rock surrounding the blast hole, explosive material, air- deck or water-deck, and stemming.

The SPH region encompasses a cylindrical rock mass with a diameter of 3 m and a height of 6 m, including stemming explosive charge, and air-deck or water-deck column at the bottom of the blast hole. Within this cylinder, a 150 mm diameter blast hole was defined. The materials within the blast hole consisted of 1.5 m of steaming, a 3.7 m explosive charge, and an 80 cm air-deck or water-deck column. To model the rock mass beyond the blast hole and the surrounding environment, the FEM numerical method was employed. The FEM domain consisted of a rectangular block with dimensions of 5 m in the x-direction, 5 m in the y-direction, and 8 m in the z-direction, enveloping the SPH cylinder (Fig. 4). The dimensions of the SPH particles and FEM mesh elements in different parts of the model are presented in Table 1. It's worth noting that a non-reflecting boundary condition (*BOUNDARY_NON_REFLECTING) was implemented to prevent wave reflection back into the model and to allow waves to propagate out of the model [44].

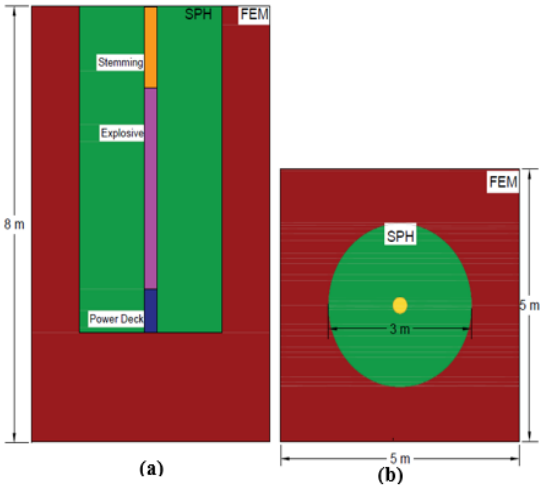

Fig. 4. Modeling of a single blast hole with bottom air-deck; a: blast hole; b: a cross-section of the blast hole.

Table 1. The SPH particle and FEM mesh size

Part	Size (mm) (SPH)	Size (mm) (FEM)
Rock	---	100
Rock	35	---
Explosive	5	---
Air-deck	5	---
Stemming	10	---

4.1. Material Models

In this study, the Barre granite rock was used to model the rock surrounding the blast. The Johnson-Holmquist (JH2) constitutive model was adopted to simulate the behavior of Barre granite rock under blast loading. This model accounts for strain rate and pressure rate effects, allowing the material to retain a residual strength after failure, even when subjected to stresses equal to its failure strength [49]. Consequently, this constitutive model exhibits excellent capability in capturing failure initiation and propagation. The JH2 model incorporates a damage model that describes the material behavior from the intact state to the fully damaged state. Additionally, this model is used to quantify the level of damage in the rock (damage parameter D, ranging from 0 to 1).

Table 2 presents the parameter values used for modeling Barre granite, using the JH2 constitutive model [49]-[51].

Table 2. JH-2 model parameters for Barre granite [49]-[51].

Parameter	Symbol	Value
Density	$\rho_\circ$ $(g.cm^{-3})$	2.66
Shear modulus (G)	G (GPa)	21.9
Intact strength coefficient (A)	A	1.25
Fractured strength coefficient (B)	B	0.68
Strain rate coefficient (C)	C	0.005
Fractured strength exponent (M)	M	0.83
Intact strength exponent (N)	N	0.68
Maximum tensile strength (T)	T (MPa)	57
Maximum normalized fractured strength	σ^*_{fmax}	0.16
Hugoniot elastic limit	HEL (GPa)	4.5
HEL pressure	PHEL (GPa)	2.93
Bulk factor	B	1.0
Damage coefficient	D1	0.008
Damage coefficient	D2	0.44
Bulk modulus	K1 (GPa)	25.7
Second pressure coefficient	K2 (GPa)	−386
Third pressure coefficient	K3 (GPa)	12800

TNT was employed as the explosive charge in the constructed model. The *MAT_HIGH_EXPLOSIVE_BURN material model available in LS-Dyna was utilized to simulate TNT [44]. The pressure generated by the explosive and the resulting detonation gases was described, using the Jones-Wilkins-Lee (JWL) equation of state, as expressed by the following equation [52]:

$$P = A_1\left(1-\frac{\omega\eta}{R_1}\right)e^{-\frac{R_1}{\eta}} + B_1\left(1-\frac{\omega\eta}{R_2}\right)e^{-\frac{R_2}{\eta}} + \omega\eta\rho_o E \quad (19)$$

Where E is the internal energy per unit volume, η is the ratio of the density of the detonation products to the initial density of the explosive, and B, R_1, R_2, and ω are material constants. The parameters for TNT used in the material model and equation of state are listed in Table 3.

Table 3. TNT parameters [53].

ρ ($g.cm^{-3}$)	VOD ($m.s^{-1}$)	Pcj (GPa)	A (GPa)	B (GPa)
1.63	6930	27	371.2	3.21
R1	R2	ω	E0($GJ.m^3$)	V0
4.15	0.95	0.3	7	1.0

In Table 3 parameters are: the density (ρ), detonation velocity (VOD), initial detonation pressure (Pcj), initial specific internal energy (E0), and initial relative volume (V0) of the explosive.

Water and air were modeled, using the MAT_NULL material model available in LS-Dyna [44]. It's important to note that a polynomial equation of state was employed to model air. This equation of state is suitable for modeling gases and represents the internal energy linearly. Additionally, the Gruneisen equation of state was used to model water. This equation of state is commonly used in LS-Dyna for modeling dense materials under high pressure. The required parameters for modeling are listed in Tables 4 and 5 [44].

Table 4. Air parameters [53].

p ($g.cm^{-3}$)	P_C	C_0	C_1	C_2	C_3
1.29×10−6	0	0	0	0	0
C_4	C_5	C_6	E_0 (MPa)	V_0	
0.4	0.4	0	0.25	0	

In Table 4, P_C is the compressive strength and C_0-C_6 are constant coefficients.

Table 5. Water parameters [54].

ρ ($kg.m^{-3}$)	Bulk sound speed CB (m·s−1)	Material constant S1
1000	1483	1.750

4.2. Validation And SPH Parameters

To validate the SPH model and determine the relevant SPH parameters, the experimental model developed by Dehghan Banadaki et al. was used as a reference [54]. The experimental model consisted of a cylindrical Barre granite rock. A blast hole was drilled at the center of the cylinder, and a detonating cord with a PTEN primary charge served as the blast source. A copper tube was inserted into the blast hole. The copper tube deformed without fracturing, effectively preventing gas penetration and the formation of cracks in the rock caused by gas expansion. Table 6 and Fig. 5 present the dimensions of the experimental model based on Dehghan Banadaki's work.

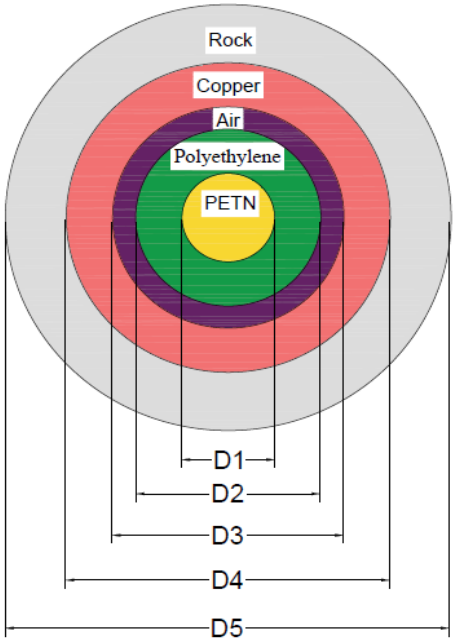

Fig. 5. The geometry of Dehghan Banadaki's experimental model [54].

Table 6. The geometry of Dehghan Banadaki's experimental model [54].

Material	Outside diameter (mm)	Symbol
PETN	1.65	D1
Polyethylene	4.5	D2
Air	5.25	D3
Copper	6.45	D4
Rock	144	--

The numerical modeling process of Dehghan Banadaki's experimental model, using the SPH numerical method and the procedure for determining the required parameters for SPH modeling is detailed in [55]. Based on this, the artificial viscosity coefficients α = 1 and β = 5 were

used for the SPH numerical modeling. Additionally, the penalty factors, as presented in Table 7, were employed in the numerical modeling of a single blast hole for simulating the air-deck blasting method.

Table 7. Penalty scale factors for different SPH parts interaction

Part interactions	Penalty scale factor
Explosive-rock	0.2
Explosive-air/water	0.8
Air/water-rock	0.8
Rock-stemming	0.2

5. RESULTS

A combined SPH-FEM numerical modeling approach was employed to simulate a single, bottom air-deck and water-deck blast hole. The influence of water presence in the uncharged bottom region of the hole was investigated. To assess the performance of the combined SPH and FEM methods and ensure accurate transmission of the blast wave at the SPH-FEM interface, the pressure at the boundary between the two regions was measured (Fig. 6). As shown in Fig. 6, the pressure exerted on the FEM region at the interface exhibits good agreement with the pressure applied to the SPH region.

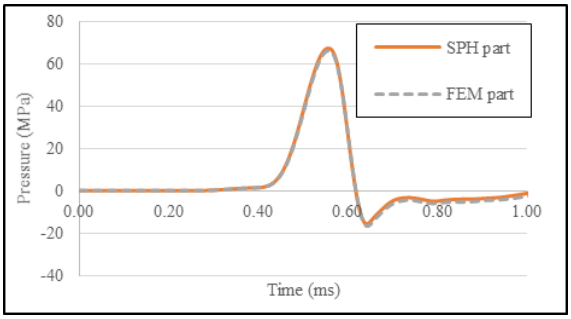

Fig. 6. Comparison of pressure measured at the SPH and FEM interface.

In air-deck blasting, the empty area at the bottom of the blast hole acts as a free face, causing the blast wave and resulting gases to rapidly propagate toward the bottom of the hole, increasing the pressure in this region [8, 25, 36, 56]. It is important to note that the pressure due to the air-deck blasting is lower than that of conventional blasting, as a smaller amount of explosive is used for the same volume. Conversely, in air-deck blasting, the blast wave is confined to the empty area at the bottom of the blast hole and oscillates. These repeated wave oscillations in the air-deck and the generation of secondary waves contribute to improved rock fragmentation [57].

To evaluate the performance of the air-deck method in both dry and water-filled hole conditions, the minimum principle stress and the pressure applied to the blast hole wall in the air-deck area for both dry and water-filled holes were measured, which are presented in Fig. 7.

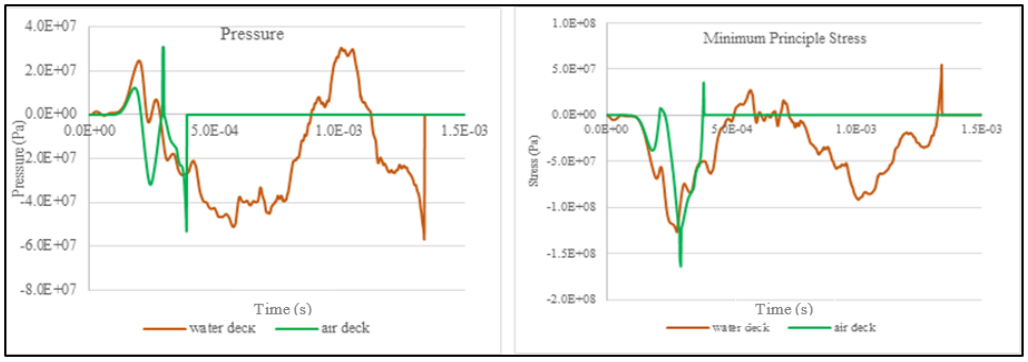

Fig. 7. Comparison of pressure and minimum principle stress in air-deck blasting and water-deck blasting.

As it can be observed from Fig. 7, the initial minimum stress applied to the blast hole wall in a water-filled hole is higher than that in a dry hole. This is due to the incompressibility of water, which transfers the applied pressure to the blast hole walls. On the other hand, over time, wave oscillations in the air-deck region under dry conditions amplify the initial wave, resulting in a stronger secondary wave in dry conditions compared to water-filled conditions. Fig. 7 clearly shows that the presence of water in the air-deck region attenuates the blast wave and reduces the frequency of the wave applied to the blast hole wall. This reduction in wave frequency causes the rock to fail at a higher stress level compared to blasting with an air-deck at the bottom of the hole. Moreover, the lower wave frequency in water-filled holes compared to dry holes leads to delayed rock failure and a longer duration of wave application to the rock. Over time, the stress applied to the blast hole wall in the air-deck area, for both water-filled and dry hole conditions, transits into tensile stress, leading to tensile failure. To investigate the rock failure mechanism

resulting from air-deck and water-deck blasting, horizontal stress was measured at a distance of 10 cm from the blast hole wall in both cases (Fig. 8). As shown in the figure, wave oscillations at the bottom of the hole and the generation of secondary tensile waves in the air-deck area are evident in both water-filled and dry hole conditions. Given that the tensile strength of rock is significantly lower than its compressive strength, the conversion of compressive waves to tensile waves in the air-deck area results in optimal fragmentation at the bottom of the hole.

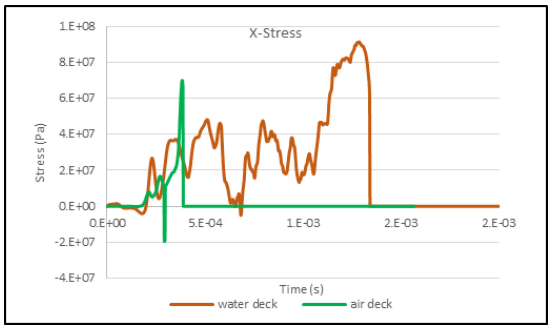

Fig. 7. Comparison of horizontal stress at a distance of 10 cm from the blast hole wall (air- deck area) in the dry model and the water-filled model.

Furthermore, the amount of energy absorbed by the rock mass under air-deck and water-deck blasting has been investigated (Fig. 9). As shown in this figure, in water- deck blasting, the energy absorbed by the rock increases rapidly at the beginning of the explosion, and then stabilizes at approximately 75 MJ. This rapid energy absorption in this blasting method is due to the incompressibility of water, which transfers the received energy to the surrounding rock. On the other hand, in the air-deck blasting, due to the presence of an empty area at the bottom of the hole, the absorption of blast energy by the rock occurs at a lower rate. However, the repeated wave oscillations in the air-deck are more pronounced and efficient compared to the water-deck. These repeated oscillations amplify the initial wave and apply the blast wave to the rock for a longer duration, resulting in a slower rate of energy absorption over time.

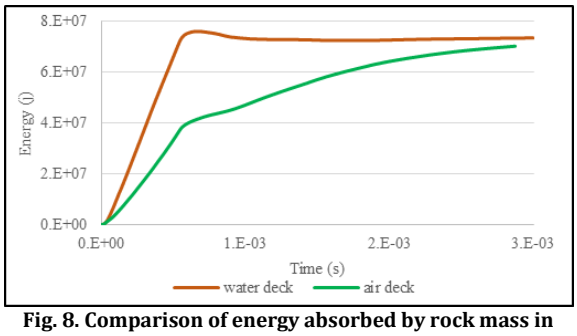

Fig. 8. Comparison of energy absorbed by rock mass in air-deck and water-deck models.

Additionally, the effective stress history at various distances from the blast hole wall resulting from air-deck and water-deck blasting was measured. The maximum effective stress in these stress histories was determined. Fig. 10 presents the maximum effective stress values measured at different distances from the blast hole wall. As shown in the figure, the maximum effective stress resulting from the blast in a water-filled hole is higher at various distances compared that in a dry hole. As previously mentioned, this is attributed to the incompressibility of water and the subsequent transfer of blast energy to the rock mass.

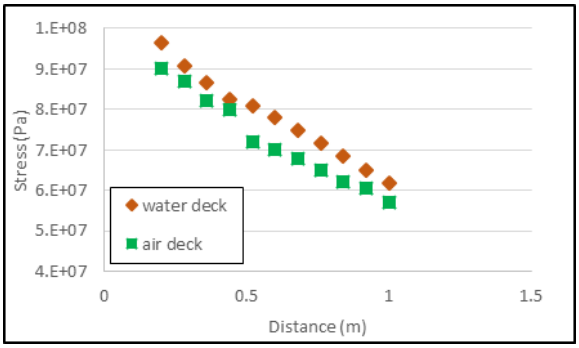

Fig. 9. Comparison of maximum effective stress taken at different distances from the blast hole wall in the air-deck, and water-deck models.

Additionally, the presence of an empty space at the bottom of the blast hole reduces the stress applied to the rock. However, as mentioned earlier, the repeated wave oscillations in the empty area amplify the initial wave and increase the duration of wave application to the rock mass. These factors contribute to improved fragmentation at the bottom of the hole, despite the reduced initial maximum stress applied to the rock mass.

Furthermore, the extent of fracturing caused by the blast in the air-deck region at the bottom of the hole was investigated under both dry and water-filled hole conditions (Fig. 11). The total fracture length in the dry and water-filled conditions was 13.15 m and 12.5 m, respectively. The small difference in fracture length between the two conditions (5%) indicates a nearly identical performance of air-deck blasting in both dry and water-filled holes. Therefore, it can be concluded that the presence of water at the bottom of the hole has a minimal impact on the blasting results, and the air-deck method can be applied to water-filled holes as well.

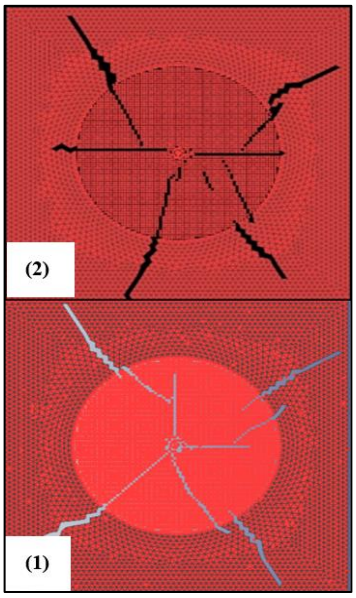

Fig. 10. Comparison of fracture due to blasting in 1) air-deck area and 2) water -deck area.

6. CONCLUSIONS

As previously mentioned, introducing an empty space at the bottom of a blast hole results in wave oscillation at the blast hole bottom, the generation of a stronger secondary wave, and repeated wave impacts on the blast hole wall, ultimately enhancing fragmentation in the bottom region of the blast hole. Conversely, in water-filled blast holes, the incompressibility of water causes the pressure exerted by the explosive to be directly transferred to the rock. Consequently, the initial pressure exerted on the blast hole while, using the water- deck is higher than that in air deck blasting. Additionally, the presence of water in the air-deck area causes attenuation of the explosive wave frequency and a reduction in wave frequency.

Wave oscillation within the air-deck area and the generation of a secondary wave in the form of a tensile wave were observed in both water-filled and dry blast holes. Since the tensile strength of rock is lower than its compressive strength, the conversion of a compressive wave into a tensile wave leads to improved rock fragmentation in the air-deck area. Moreover, due to the incompressibility of water, the transfer of explosive wave energy to the rock in the water-deck occurs at a steep gradient and in a shorter time. However, with wave oscillation in the empty space of a dry blast hole and the amplification of the primary wave, the transfer of the basting wave in a dry blast hole occurs at a lower speed and with a gentler gradient, which contributes to more uniform rock fragmentation.

On the other hand, measurements of the maximum effective stress at various distances around the blast hole and in the air-deck area revealed that the maximum stress induced in the rock is higher in water-filled blast holes, as the blasting energy is transferred to the rock through water in this method. However, in air-deck blasting, the initial pressure exerted on the rock is lower. Additionally, the repeated wave oscillation in the air-deck area and the amplification of the primary wave contribute to improved fragmentation. This was evident in the fractures induced by the blast in the air-deck area. Fractures in the air-deck area of dry blast holes were only 5% more than those in water-filled blast holes. Therefore, it can be concluded that the presence of water at the bottom of the blast hole has a minimal impact on the results of blasting with the deck at the bottom of the blast hole, and the air-deck method can be employed in water-filled blast holes.

REFERENCES

[1] Ozer, U. (2008). Environmental impacts of ground vibration induced by blasting at different rock units on the Kadikoy–Kartal metro tunnel. Engineering geology, 100(1-2), 82-90.

[2] Jhanwar, J. C., Jethwa, J. L., & Reddy, A. H. (2000). Influence of air-deck blasting on fragmentation in jointed rocks in an open-pit manganese mine. Engineering Geology, 57(1-2), 13-29.

[3] Jhanwar, J. C., & Jethwa, J. L. (2000). The use of air decks in production blasting in an open pit coal mine. Geotechnical & Geological Engineering, 18, 269-287.

[4] Sazid, M., & Singh, T. N. (2013, May). Mechanism of air deck technique in rock blasting-a brief review. In Fourth Indian Rock Conference, no. May (pp. 29-31).

[5] Jhanwar, J. C. (2011). Theory and practice of air-deck blasting in mines and surface excavations: a review. Geotechnical and Geological Engineering, 29(5), 651-663.

[6] Rowlands, M. D. (1991, November). Separating explosive charges with air gaps to improve fragmentation whilst reducing explosive usage: Proc 2nd Conference on Large Open Pit Mining, Latrobe Valley, 3–6 April 1989 P105–107. Publ Melbourne: AusIMM, 1989. In International Journal of Rock Mechanics and Mining Sciences & Geomechanics Abstracts (Vol. 28, No. 6, p. A371). Pergamon.

[7] Correa, C. E. (2003). Use of air-decks to reduce subdrillings in Escondida mine. Fragblast, 7(2), 79-86.

[8] Chiappetta, R. F. (2004). New blasting technique to eliminate subgrade drilling, improve

fragmentation, reduce explosive consumption and lower ground vibrations. Journal of explosives engineering, 21(1), 10-12.

[9] Floyd, J. (2004). Power deck optimization. Power Deck Company. Blast Dynamics.

[10] Askari Badoee, M. J., Ebrahimi Farsangi, M. A., Mansouri, H., & Mansour Panahi, A. M. (2018). Application of power-deck in wet candition, case study, Goharzamin iron ore mine. 12th International Symposyom on Rock Fragmentatin by Blasting.

[11] Zarei, M., Shahabi, R. S., Hadei, M. R., & Louei, M. Y. (2022). The use of air decking techniques for improving surface mine blasting. Arabian Journal of Geosciences, 15(19), 1545.

[12] Zhu, Z., Mohanty, B., & Xie, H. (2007). Numerical investigation of blasting-induced crack initiation and propagation in rocks. International Journal of Rock Mechanics and Mining Sciences, 44(3), 412-424.

[13] Bendezu, M., Romanel, C., & Roehl, D. (2017). Finite element analysis of blast-induced fracture propagation in hard rocks. Computers & Structures, 182, 1-13.

[14] Gui, Y. L., Bui, H. H., Kodikara, J., Zhang, Q. B., Zhao, J., & Rabczuk, T. (2016). Modelling the dynamic failure of brittle rocks using a hybrid continuum-discrete element method with a mixed-mode cohesive fracture model. International Journal of Impact Engineering, 87, 146-155.

[15] Rabczuk, T., Zi, G., Bordas, S., & Nguyen-Xuan, H. (2010). A simple and robust three-dimensional cracking-particle method without enrichment. Computer Methods in Applied Mechanics and Engineering, 199(37-40), 2437-2455.

[16] Rabczuk, T., & Belytschko, T. (2004). Cracking particles: a simplified meshfree method for arbitrary evolving cracks. International journal for numerical methods in engineering, 61(13), 2316-2343.

[17] Rabczuk, T., & Belytschko, T. (2007). A three-dimensional large deformation meshfree method for arbitrary evolving cracks. Computer methods in applied mechanics and engineering, 196(29-30), 2777-2799.

[18] Rabczuk, T., Bordas, S., & Zi, G. (2010). On three-dimensional modelling of crack growth using partition of unity methods. Computers & structures, 88(23-24), 1391-1411.

[19] Fan, H., Bergel, G. L., & Li, S. (2016). A hybrid peridynamics–SPH simulation of soil fragmentation by blast loads of buried explosive. International Journal of Impact Engineering, 87, 14-27.

[20] Morris, J. P., Rubin, M. B., Block, G. I., & Bonner, M. P. (2006). Simulations of fracture and fragmentation of geologic materials using combined FEM/DEM analysis. International Journal of Impact Engineering, 33(1-12), 463-473.

[21] Fakhimi, A., & Lanari, M. (2014). DEM–SPH simulation of rock blasting. Computers and Geotechnics, 55, 158-164.

[22] Xu, J. X., & Liu, X. L. (2008). Analysis of structural response under blast loads using the coupled SPH-FEM approach. Journal of Zhejiang University-SCIENCE A, 9(9), 1184-1192.

[23] Gharehdash, S., Shen, L. M., Gan, Y. X., & Flores-Johnson, E. A. (2016). Numerical investigation on fracturing of rock under blast using coupled finite element method and smoothed particle hydrodynamics. Applied Mechanics and Materials, 846, 102-107..

[24] Ning, Y., Yang, J., An, X., & Ma, G. (2011). Modelling rock fracturing and blast-induced rock mass failure via advanced discretisation within the discontinuous deformation analysis framework. Computers and Geotechnics, 38(1), 40-49.

[25] Wang, Z. L., Li, Y. C., & Shen, R. F. (2007). Numerical simulation of tensile damage and blast crater in brittle rock due to underground explosion. International Journal of Rock Mechanics and Mining Sciences, 44(5), 730-738.

[26] Liu, M. B., & Liu, G. (2010). Smoothed particle hydrodynamics (SPH): an overview and recent developments. Archives of computational methods in engineering, 17, 25-76.

[27] Gingold, R. A., & Monaghan, J. J. (1977). Smoothed particle hydrodynamics: theory and application to non-spherical stars. Monthly notices of the royal astronomical society, 181(3), 375-389.

[28] Vignjevic, R., & Campbell, J. (2009). Review of development of the smooth particle hydrodynamics (SPH) method. In Predictive modeling of dynamic processes: a tribute to professor Klaus Thoma (pp. 367-396). Boston, MA: Springer US.

[29] Feng, Y., Jianming, W., & Feihong, L. (2012). Numerical simulation of single particle acceleration process by SPH coupled FEM for abrasive waterjet cutting. The International Journal of Advanced Manufacturing Technology, 59, 193-200.

[30] Rabczuk, T., & Eibl, J. (2003). Simulation of high velocity concrete fragmentation using SPH/MLSPH. International Journal for Numerical Methods in Engineering, 56(10), 1421-1444.

[31] Hu, Y., Lu, W., Chen, M., Yan, P., & Zhang, Y. (2015). Numerical simulation of the complete rock blasting response by SPH–DAM–FEM approach. Simulation Modelling Practice and Theory, 56, 55-68.

[32] Gharehdash, S., Shen, L. M., Gan, Y. X., & Flores-Johnson, E. A. (2016). Numerical investigation on fracturing of rock under blast using coupled finite element method and smoothed particle

hydrodynamics. Applied Mechanics and Materials, 846, 102-107.

[33] Wang, Z. L., Huang, Y. P., Li, S. Y., & Xiong, F. (2020, October). SPH-FEM coupling simulation of rock blast damage based on the determination and optimization of the RHT model parameters. In IOP conference series: earth and environmental science (Vol. 570, No. 4, p. 042035). IOP Publishing.

[34] Melnikov, N. V., & Marchenko, L. N. (1970, November). Effective methods of application of explosion energy in mining and construction. In ARMA US Rock Mechanics/Geomechanics Symposium (pp. ARMA-70). ARMA.

[35] Mel'Nikov, N. V., Marchenko, L. N., Zharikov, I. F., & Seinov, N. P. (1979). A method of enhanced rock breaking by blasting. Soviet Mining, 15(6), 565-572.

[36] Hayat, M. B., Alagha, L., & Ali, D. (2019). Air decks in surface blasting operations. Journal of Mining Science, 55, 922-929.

[37] Moxon, N. T., Mead, D., & Richardson, S. B. (1993). Air-decked blasting techniques: some collaborative experiments. Transactions of the Institution of Mining and Metallurgy. Section A. Mining Industry, 102.

[38] Lucy, L. B. (1977). A numerical approach to the testing of the fission hypothesis. Astronomical Journal, vol. 82, Dec. 1977, p. 1013-1024., 82, 1013-1024.

[39] Liu, G. R., & Liu, M. B. (2003). Smoothed particle hydrodynamics: a meshfree particle method. World scientific.

[40] Nguyen, V. P., Rabczuk, T., Bordas, S., & Duflot, M. (2008). Meshless methods: a review and computer implementation aspects. Mathematics and computers in simulation, 79(3), 763-813.

[41] Liu, G. R., & Liu, M. B. (2003). Smoothed particle hydrodynamics: a meshfree particle method. World scientific.

[42] Libersky, L. D., Randles, P. W., Carney, T. C., & Dickinson, D. L. (1997). Recent improvements in SPH modeling of hypervelocity impact. International Journal of Impact Engineering, 20(6-10), 525-532.

[43] Vignjevic, R., De Vuyst, T., Campbell, J. C., & Source, C. (2006). A frictionless contact algorithm for meshless methods. Computer Modeling in Engineering and Sciences, 13(1), 35.

[44] LS-DYNA. (2015). Keyword user's manual, Version R9.0.1. Livermore, CA. Livermore Software Technology Corporation.

[45] Gharehdash, S., Barzegar, M., Palymskiy, I. B., & Fomin, P. A. (2020). Blast induced fracture modelling using smoothed particle hydrodynamics. International Journal of Impact Engineering, 135, 103235.

[46] Swegle, J. W., Hicks, D. L., & Attaway, S. W. (1995). Smoothed particle hydrodynamics stability analysis. Journal of computational physics, 116(1), 123-134.

[47] Koneshwaran, S., Thambiratnam, D. P., & Gallage, C. (2015). Performance of buried tunnels subjected to surface blast incorporating fluid-structure interaction. Journal of Performance of Constructed Facilities, 29(3), 04014084.

[48] Jhanwar, J. C. (1998). Investigation into air-deck blasting and its influence on blast performance and economics in open-pit mines. Unpublished ME Thesis, Department of Mining Engineering, Visvesvaraya Regional College of Engineering, Nagpur University, Nagpur, India, 142.

[49] Johnson, G. R., & Holmquist, T. J. (1999). Response of boron carbide subjected to large strains, high strain rates, and high pressures. Journal of applied physics, 85(12), 8060-8073.

[50] Ai, H. A., & Ahrens, T. J. (2006). Simulation of dynamic response of granite: A numerical approach of shock-induced damage beneath impact craters. International Journal of Impact Engineering, 33(1-12), 1-10.

[51] Ma, G. W., & An, X. M. (2008). Numerical simulation of blasting-induced rock fractures. International Journal of Rock Mechanics and Mining Sciences, 45(6), 966-975.

[52] Dobratz, B. M. (1972). Properties of chemical explosives and explosive simulants (No. UCRL-51319; UCRL-51319 (REV. 1)). comp. and ed.; Lawrence Livermore National Lab.(LLNL), Livermore, CA (United States).

[53] Banadaki, M. D., & Mohanty, B. (2012). Numerical simulation of stress wave induced fractures in rock. International Journal of Impact Engineering, 40, 16-25.

[54] Banadaki, M. M. D. (2010). Stress-wave induced fracture in rock due to explosive action (p. 128). Toronto: University of Toronto.

[55] Moradi, M., Mansouri, H., Ebrahimi Farsangi, M. A., & Saffari Pour, M. (2024). Modelling of bottom air-deck blasting in a Single Hole, Using the SPH–FEM Method. Geotechnical and Geological Engineering, 1-21.

[56] Thote, N. R., & Singh, D. P. (2000). Effect of airdecking on fragmentation: A few case studies of Indian mining. Explosives and Blasting Technique. Rotterdam.

[57] Chiappetta, R. F. (1992, June). Precision detonators and their applications in improving fragmentation, reducing ground vibrations and increasing reliability—a look into the future. In Proceeding of 4th high tech seminar blasting technology instrumentation and explosives applications. Tennessee (pp. 1-39).